PNAS
www.pnas.org

Supplementary Information for

Ballistic thermal phonons traversing nanocrystalline domains in oriented polyethylene

Andrew B. Robbins, Stavros X. Drakopoulos, Ignacio Martin-Fabiani, Sara Ronca, and Austin J. Minnich

Austin J. Minnich
E-mail: aminnich@caltech.edu

This PDF file includes:

Supplementary text
Figs. S1 to S3
References for SI reference citations

Supporting Information Text

S1. Sample Fabrication

Here we include additional information pertaining to sample fabrication.

Compression molding. Completely sintered 5 cm x 6 cm slabs were made by applying a load of 5 tons for 5 min, 10 tons for 10 min, and 20 tons for 5 min, all at 125 °C, below the melting temperature (∼140 °C). During cooling, between 1 and 5 tons were applied to achieve permanent deformation(1).

Calendering. The samples were uniaxially oriented by means of twin-rolling at a speed of 0.1 rpm and 125 °C. For each specimen, the process lasted approximately 45 minutes. Calendering induces uniform orientation throughout the slab so the draw ratio was calculated by measuring the initial and final length of the slab.

S2. Wide-Angle X-ray Scattering (WAXS)

Here we include raw data from WAXS measurements in Figure S2, along with measurements of the FWHM of the (200) peaks and the corresponding calculations for crystallinity in Figure S3.

S3. Transient Grating (TG)

Data Fitting and Analysis. While the thermal signals discussed in the main text can be fit to an exponential decay, additional non-thermal signals are sometimes present in measured data that appear as additional exponential decays. One potential source of a non-thermal signal is the thermalization process in the dye or filler. These decays are typically very fast relative to the thermal signal and do not impact the sensitivity of the main thermal decay, τ. Another non-thermal signal that is sometimes observed is an exponential with slow decay times relative to the thermal decay. This signal was observed in some data for DR7.5 and a separate exponential decay is incorporated into the fitting procedure to account for it. The source of this signal is likely heterogeneous light scattering introduced at higher draw ratios. The overall light transmission can be very sensitive to location on the sample, resulting in small magnitude variations from minor movements in the sample that may result from the pump excitation. These decay constants were slow enough relative to the thermal decay timescales to ensure sufficient sensitivity of τ in the fitting procedure, and the magnitude of this signal was typically close to an order of magnitude lower than the thermal signal.

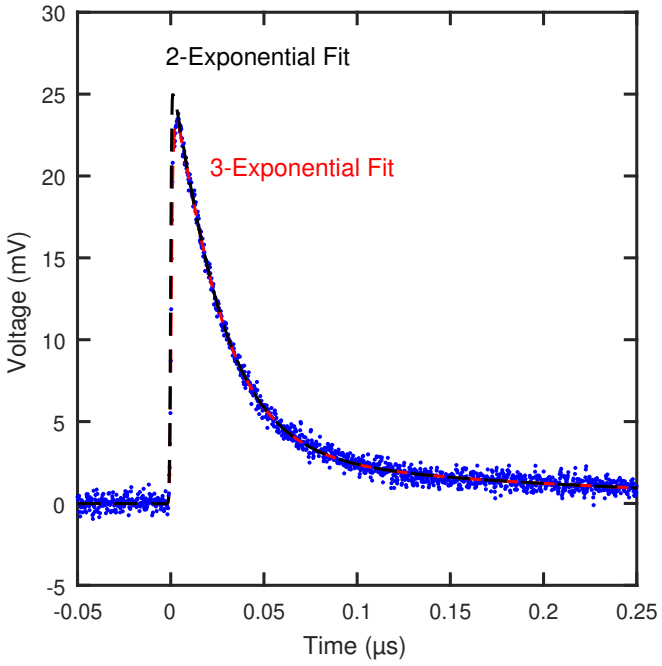

Fig. S1. Example of fitting a transient grating signal from DR7.5 with ZnO fillers, for a grating period of 2.29 μm. The full fit is shown in red, which is composed of 3 exponential decays, with decay times 24.9 ns (thermal decay), 890 ps (fast decay), and 272 ns (slow decay). The fitting shown in black includes only the thermal decay and the slow decay.

As an example, Figure S1 shows a transient grating signal taken on DR7.5 with ZnO fillers, using a grating period of 2.29 μm. The data shown is best fit using 3 exponentials, shown in the plot in red, including the primary thermal decay, a short decay, and a long decay. The fitting shown in black leaves out the short decay for demonstration purposes only, showing that its presence is necessary to capture the signal's behavior immediately after time $t = 0$. However, comparing the two fits also

demonstrates that the fast decay is sufficiently fast and low magnitude that it does not affect the primary thermal exponential decay. This confirms that the fitting has the appropriate sensitivity to the thermal decay. Finally, the slow decay, which is more than 10 times slower than the thermal decay, can be seen as the small slope approaching 0 at the end of the signal. This low magnitude decay also does not significantly affect the fitting's sensitivity for the thermal decay. The magnitude of this slow decay can vary for different measured data, however the magnitude was always observed to be low relative to the main exponential, sometimes not being noticeably present at all.

Error Analysis. The error bars in this work represent the combination of two independent error sources. The first source is the standard error that is output from the nonlinear least squares regression implemented in MATLAB's Statistics and Machine Learning Toolbox. The second source accounts for variation across the sample and was calculated by comparing fitted thermal conductivity values from 8 independent measurements on S7.5 at a grating period of $d = 6.4\,\mu\text{m}$, taken at different sample locations at different times. The standard deviation of these measurements was found to be 3.5% of the mean value. This fractional variation was extrapolated to all samples. The variance of the two error sources is added to calculate the error bar for each data point.

S4. MFP Reconstruction

MFP reconstruction is carried out using Bayesian inference. Similar to Ravichandran et al.(2), we use the Metropolis-Hastings Markov chain Monte Carlo algorithm to generate a distribution of possible MFP accumulation functions ($F(\Lambda)$) that are most likely to describe the measurements. The algorithm is given in Algorithm 1.

Algorithm 1 Metropolis-Hastings Markov chain Monte Carlo

1: Choose an initial F_0 ▷ vector length M
2: **for** $i = 1, ..., N$ **do**
3: Choose new sample F_i from $K(F|F_{i-1})$ ▷ Sample proposal distribution
4: Evaluate $\pi(F_i) = P_{like}(\kappa|F_i) \times P_{prior}(F_i)$ ▷ Evaluate posterior probability
5: Compute the acceptance probability

$$\alpha(F_i, F_{i-1}) = \textbf{min}\left[1, \frac{\pi(F_i)}{\pi(F_{i-1})}\right]$$

6: Accept F_i with a probability equal to α. If rejected, set $F_i = F_{i-1}$

According to this framework, an initial guess for $F(\Lambda)$, denoted F_0, is chosen as the initial sample. This vector consists of M elements, one at each discretized MFP point.

Then, a new sample is chosen according to a proposal distribution, $K(F|F_{i-1})$. A common choice for K is a normal distribution, which varies the individual elements of F by small amounts on each iteration. However, F has some constraints that must be considered. First, F must always be positive, and second, it must be monotonically increasing. These constraints follow from it being an accumulation function. As a result, instead of F, we consider first the differential thermal conductivity function f, equal to the derivative of F. With this choice, as long as f is positive, F must be monotonically increasing. Second, we consider $g = \log(f)$. This ensures f will always be positive, thereby satisfying all of our constraints.

Finally, we make one more modification to our proposal distribution to increase the efficiency of the algorithm. As discussed by Ravichandran et al.(2), a prior distribution is chosen to enforce smoothness. As given, the proposal distribution independently varies each element by some quantity, Δg_j, meaning any two adjacent points have a 50% chance of having opposite sign and therefore making a smooth part of the curve less smooth. To counteract this change, we define $\Delta g'_j$:

$$\Delta g'_j = \sum_{j'}^{M} \Delta g_{j'} \exp\left(-\frac{((j-j')\Delta\Omega)^2}{2\sigma_s^2}\right) \quad [1]$$

where we effectively smooth out the independent Δg_j terms by adding contributions from neighboring terms, weighted with a Gaussian distribution. Here, $\Delta\Omega$ is the distance in log space between neighboring MFP points and σ_s is a smoothing constant. This modification to the proposal distribution algorithm has no effect on the final outcome, but merely confers a benefit in computational efficiency.

Resuming the steps in Algorithm 1, once the next sample is found, the posterior probability is computed proportional to both the likelihood that the sample explains the data and the value of the prior distribution. This step is identical to Ravichandran et al.(2). And the likelihood function is specifically evaluated by computing thermal conductivity values from the sample, F, according to previous works by Minnich(3, 4).

The prior distribution, defined as:

$$P(F) \propto \exp\left(-\frac{1}{2\gamma^2}\sum_{j}^{M} W_j^2 \Delta\Omega\right) \quad [2]$$

has a γ term that can adjust the smoothness constraint. For example, when $\gamma = 0$, perfect smoothness is required. When $\gamma = \infty$, there is no constraint on smoothness. Because there is no a priori way to choose a value for γ, we varied γ over a range of values, including low values (0.1) where the prior restricted the solution to be a straight line, as well as high values (10) where the solution became independent of γ. We then conducted a MC simulation where γ was smoothly varied (in log space) so that the final posterior distribution includes contributions from a wide range of γ values. While this conservative procedure leads to larger degrees of uncertainty in the final posterior distribution, it does not require an arbitrary γ.

Finally, the algorithm incorporates an acceptance probability that rejects points with low posterior probabilities, causing the Markov chain to selectively sample volumes of parameter space with higher probability values. The algorithm is repeated N times, where N is empirically chosen to be larger enough to reach convergence. We used $N \geq 1 \times 10^8$. Additionally, we used a "burn-in" period of 1×10^5 where the algorithm was running, but no results were being saved. This procedure ensured that the Markov chain was able to find and occupy the appropriate region of parameter space prior to computing distributions.

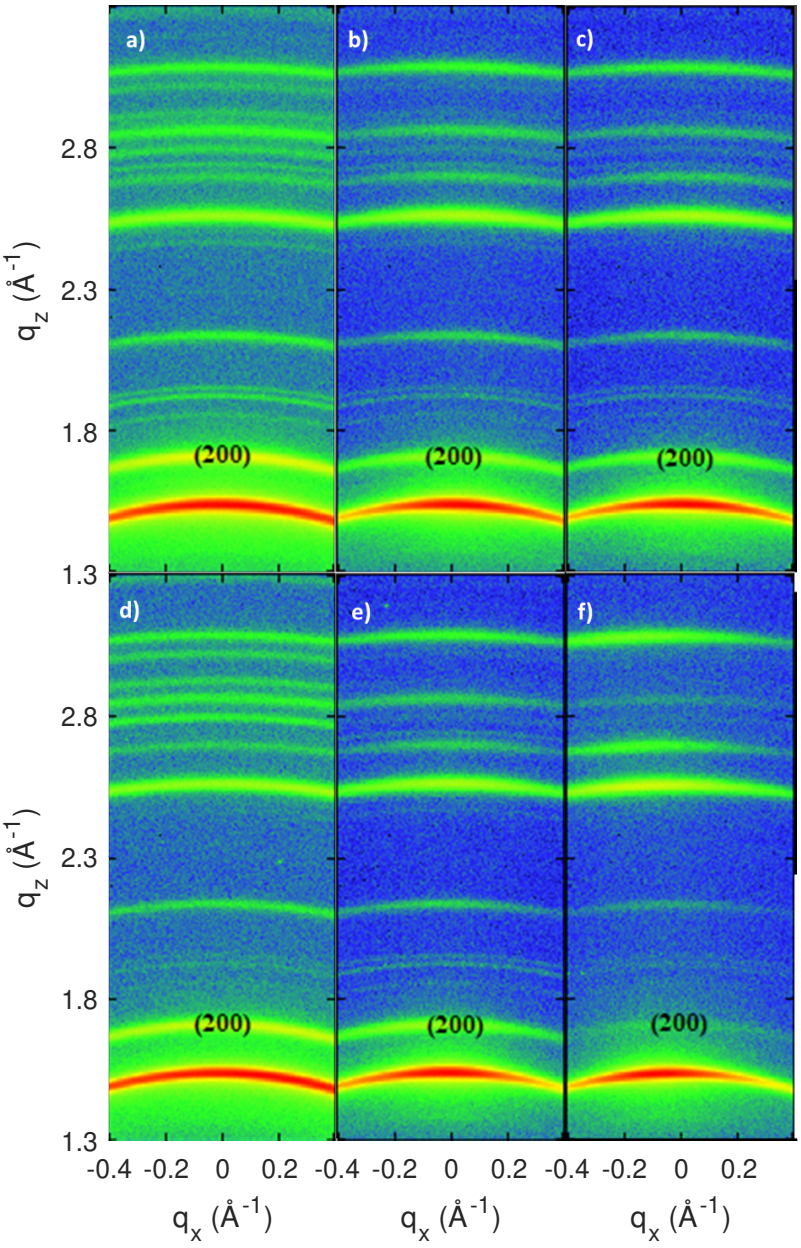

Fig. S2. 2D WAXS patterns for films with (a-c) beta-carotene and (d-f) ZnO fillers. From left to right, the draw ratios are 2.5, 5.0 and 7.5.

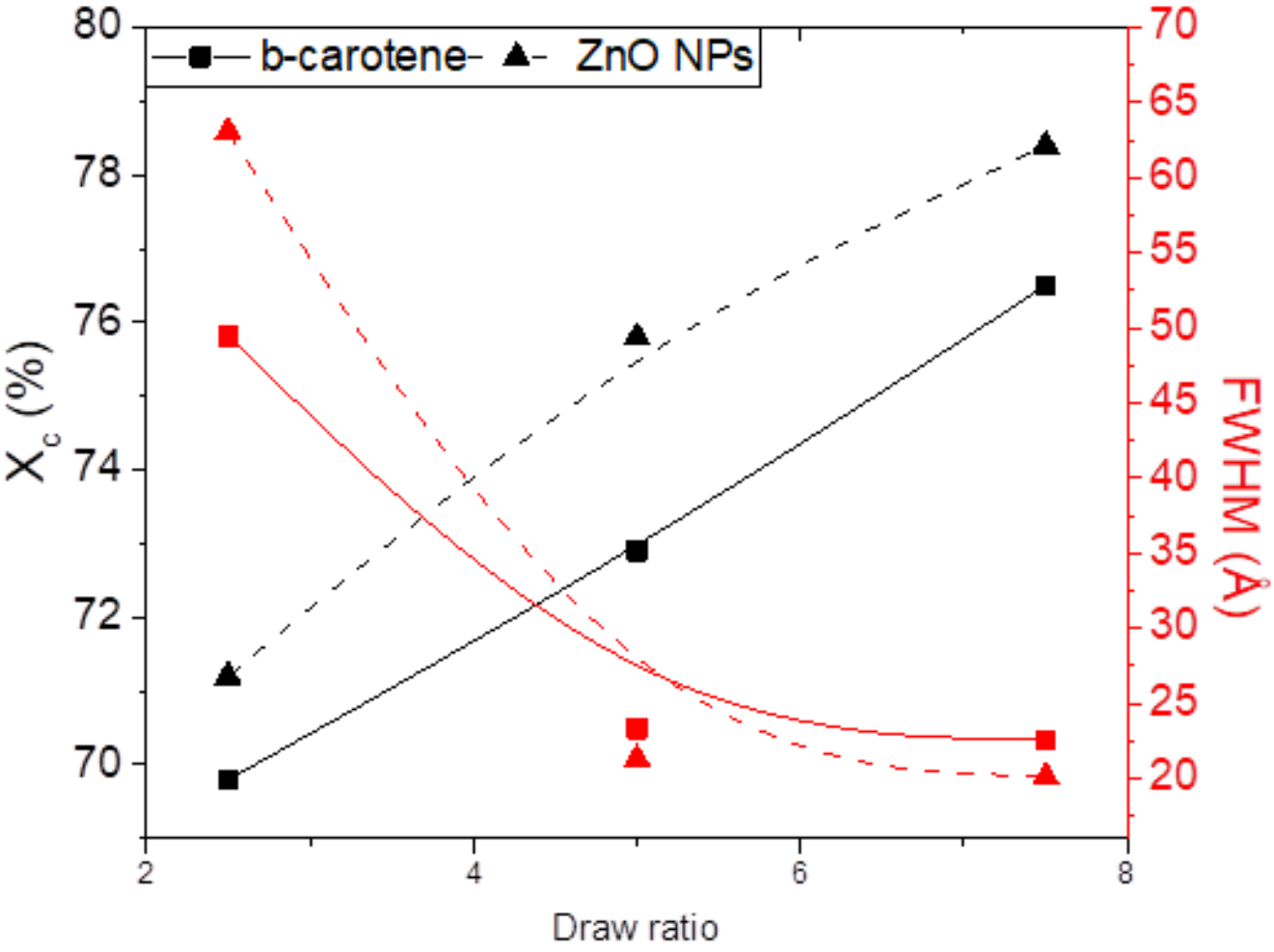

Fig. S3. Left axis: Crystallinity X_c as calculated from the reduced 1D WAXS profiles obtained from the azimuthal integration of the 2D patterns in Figure S2. Right axis: Full-width at half maximum (FWHM) as obtained by radial integration over a narrow q range around the (200) reflection and Lorentzian fitting of the resulting azimuthal profile. The lines are a guide for the eye.

References

1. Drakopoulos SX, Psarras GC, Forte G, Martin-Fabiani I, Ronca S (2018) Entanglement dynamics in ultra-high molecular weight polyethylene as revealed by dielectric spectroscopy. *Polymer* 150:35–43.
2. Ravichandran NK, Zhang H, Minnich AJ (2018) Spectrally Resolved Specular Reflections of Thermal Phonons from Atomically Rough Surfaces. *Physical Review X* 8(4):041004.
3. Minnich AJ (2012) Determining Phonon Mean Free Paths from Observations of Quasiballistic Thermal Transport. *Physical Review Letters* 109(20):205901.
4. Minnich AJ (2015) Phonon heat conduction in layered anisotropic crystals. *Physical Review B* 91(8):085206.